

Satellite-Based Nowcasting of West African Mesoscale Storms Has Skill at up to 4-h Lead Time

R. R. BURTON,^a A. M. BLYTH,^a Z. CUI,^a J. GROVES,^a B. L. LAMPTEY,^b J. K. FLETCHER,^c J. H. MARSHAM,^c D. J. PARKER,^c AND A. ROBERTS^c

^a National Centre for Atmospheric Science, Leeds, United Kingdom

^b West African Science Service Centre on Climate Change and Adapted Land Use, Accra, Ghana

^c Institute for Climate and Atmospheric Science, University of Leeds, United Kingdom

(Manuscript received 31 March 2021, in final form 19 November 2021)

ABSTRACT: The ability to predict heavy rain and floods in Africa is urgently needed to reduce the socioeconomic costs of these events and increase resilience as climate changes. Numerical weather prediction in this region is challenging, and attention is being drawn to observationally based methods of providing short-term nowcasts (up to ~6-h lead time). In this paper a freely available nowcasting package, pySTEPS, is used to assess the potential to provide nowcasts of satellite-derived convective rain rate for West Africa. By analyzing a large number of nowcasts, we demonstrate that a simple approach of “optical flow” can have useful skill at 2-h lead time on a 10-km scale and 4-h lead time at larger scales (200 km). A diurnal variation in nowcast skill is observed, with the worst-performing nowcasts being those that are initialized at 1500 UTC. Comparison with existing nowcasts is presented. Such nowcasts, if implemented operationally, would be expected to have significant benefits.

SIGNIFICANCE STATEMENT: A freely available, easy-to-use nowcasting package has been applied to satellite-retrieved rainfall rates for West Africa, and extrapolations have useful skill at up to 4 h of lead time.

KEYWORDS: Cloud tracking; Satellite observations; Mesoscale systems; Africa; Nowcasting


1. Introduction

There is an urgent need for improved predictions of high-impact weather in Africa, particularly of heavy rain and floods. According to the United Nations Office for the Coordination of Humanitarian Affairs, in 2020 alone flooding affected 1.7 million people in West and Central Africa, with many regions recording excessive rainfall (UNOCHA 2020). These floods affect lives and livelihoods, housing, and agriculture. The ability to predict the storms that cause such events is thus of great importance. Numerical weather prediction (NWP) is inherently challenging in the tropics where the Coriolis force is weak, weather is dominated by moist convection, and there are relatively few in situ observations for assimilation into models (Žagar 2017; Marsham et al. 2013; Kniffka et al. 2020; Judt 2020). Vogel et al. (2020) examined state-of-the-art ensemble predictions of rainfall over tropical Africa from the European Centre for Medium-Range Weather Forecasts (ECMWF) and compared them with an extended probabilistic climatology ensemble (Vogel et al. 2018) based on the years 1998–2017. They found that over tropical Africa only 19% of grid points in ECMWF ensembles showed skill. They found some improvement in postprocessing the ensembles,

but “over the cores of the oceanic deserts and tropical Africa skill remains close to zero.”

Given the challenges facing NWP in this region, near-real-time, observationally based solutions are needed. Nowcasting is the very-near-term prediction of high-impact weather, based in the use of near-real-time observations, with typical lead times of 0 to at most 6 h (Battrick and Mort 1981; Browning 1982; Wang et al. 2017; Roberts et al. 2021). It provides a complementary approach to NWP, because nowcasting exploits the availability of observations to provide more accurate predictions in the very near term than NWP can. Furthermore, nowcasting can provide information before the most recent initializations of NWP are available, or at lead times when model spinup can lead to poor rainfall prediction.

Ideas of nowcasting were developed for ground-based radar outside Africa (e.g., Golding 1998) and have been used in other parts of the world too (Bowler et al. 2006; Woo and Wong 2017). Automated nowcasting systems incorporating radar data are in place globally—Wang et al. (2017, their Table 2.3) lists 14 such systems. For sub-Saharan Africa, the extremely sparse radar coverage outside of South Africa and the challenges in maintaining radars mean that there is an opportunity for nowcasting based on retrievals from geostationary satellites (Roberts et al. 2021). The large, long-lived storms that provide the bulk of the rainfall to many areas of West Africa appear particularly well suited to satellite-based nowcasting, since mature systems are clearly visible from space and last many hours, or even days (Maranan et al. 2018). One of the earliest indications that satellite data could be useful in nowcasting was Birkenheuer (1987), who

 Denotes content that is immediately available upon publication as open access.

Corresponding author: Ralph Burton, ralph.burton@ncas.ac.uk

DOI: 10.1175/WAF-D-21-0051.1

© 2022 American Meteorological Society. For information regarding reuse of this content and general copyright information, consult the AMS Copyright Policy (www.ametsoc.org/PUBSReuseLicenses).

investigated the benefits of animations of satellite data. These animations allowed the forecaster to infer cloud motion—an intuitive version of the mathematical methods described below in section 3. Subsequently, nowcasting techniques using geostationary satellites have received widespread interest (Mecikalski and Bedka 2006; Bedka et al. 2010; Sieglaff et al. 2013; Line et al. 2016). More recently, studies have investigated the potential of using data assimilation (Otsuka et al. 2019) and machine-learning techniques in satellite nowcasting (see, e.g., Shi et al. 2017; Lebedev et al. 2019).

Despite the need and opportunity for satellite-based nowcasting there is very little operational nowcasting in sub-Saharan Africa. The rare examples include the nowcasting work performed by the South African Weather Service (de Coning et al. 2015; Gijben and De Coning 2017) and the promising study of Thiery et al. (2017), who proposed satellite observations as a means of indicating thunderstorm risks over Lake Victoria. There is almost no use of automated tools outside of South Africa (Roberts et al. 2021).

The European Organization for the Exploitation of Meteorological Satellites (EUMETSAT) have developed a number of satellite-based nowcast products (EUMETSAT 2021; NWCSAF 2020). Since March 2019 the Global Challenges Research Fund (GCRF) Science for Weather and Forecasting Techniques (SWIFT) project has been generating satellite-based nowcast products for Africa and working with African centers to support local generation of such products. The default settings of these satellite-based nowcasts give a forward extrapolation of 60 min, but Hill et al. (2020) found that they exhibited skill relative to persistence for up to 90 min and suggested that there was good potential for further skillful extrapolation. Comparison with these already existing nowcasts is presented in section 5c.

In summary, West Africa is a region where global NWP is challenging. Although geostationary satellite data have their own problems (see below, section 2), coverage by such satellites is excellent and the longevity of storms means that nowcasting has the potential to usefully predict storm behavior into the future, conceivably for several hours. The aim of this paper is to demonstrate the potential of satellite nowcasting for West African storms by means of free and self-contained software, that is both easy and inexpensive to run, and to evaluate the limits of useful forward projection that may be achieved.

This paper is structured as follows. In section 2, the satellite data are described. Section 3 presents the pySTEPS software and optical flow method, with some example nowcasts; section 4 describes the verification algorithm. The data selection and quality control of the satellite data are given in section 5, and results are given in section 6. These include a statistical summary of the pySTEPS nowcasts performed for this paper and comparison with the existing nowcasts described above.

2. Description of the CRR dataset

Convective rain rate (CRR; Hernanz and Lahuerta 2019) is a satellite-derived product that represents an estimate of convective rainfall from a combination of the infrared ($10.8 \mu\text{m}$),

water vapor ($6.2 \mu\text{m}$), and visible ($0.6 \mu\text{m}$) wavelength channels from the Meteosat Second Generation (MSG) Spinning Enhanced InfraRed Imager (SEVIRI) instrument (SEVIRI 2021; NWCSAF 2020). Essentially, the CRR algorithm reflects the empirical relationship that the higher and thicker the detected clouds, the higher the probability and intensity of precipitation (Hernanz and Lahuerta 2019). With a temporal resolution of 15 min and a spatial resolution of approximately 4 km, CRR has been found to be a useful product by African forecasters (Hill et al. 2020). It is produced in near-real time, has skill in identifying rainfall events in near-real time (Hill et al. 2020), is distributed pre-computed on the EUMETCast Africa service, and is a product that can be processed by the software used in this paper (see section 3).

Forward extrapolations of CRR are already available (Jann 2017; Hill et al. 2020). In the original Nowcasting Satellite Application Facility (NWCSAF) extrapolation algorithm, the position of a pixel at the next time step is determined by the atmospheric motion vector (AMV) interpolated onto the pixel grid. Then the new position of the pixel, P2, is extrapolated with the AMV that had been retrieved at position P1. A trajectory is produced by repeating the above procedure. The smoothed trajectory field is then applied to the rain rate field. Assumptions made within this NWCSAF framework include (i) the interpolated AMV at a pixel grid is produced by an inverse displace weighted interpolation scheme, (ii) the AMV used for the next position of a pixel is assumed to be persistent, (iii) the displacement field is supposed to be temporally invariable in producing the trajectory, and (iv) the trajectory field is smoothed. The recommended maximum lead time for these NWCSAF extrapolations is 60 min (Hill et al. 2020).

The NWCSAF CRR extrapolations have been recently evaluated against the high-quality microwave-only Integrated Multi-satellitE Retrievals for Global Precipitation Measurement (IMERG) satellite rainfall product in Hill et al. (2020). They found that the skill of NWCSAF CRR extrapolations is similar to the skill of the CRR retrievals themselves: there is considerably higher skill than climatology, but there is a large difference in skill between day, when information from visible channels is available, and night.

Data selection and quality control

The CRR dataset was subject to the following criterion: for each of the initialization start times of (0000, 0300, ..., 2100 UTC) there must exist three frames prior to the start of the nowcast, spaced 15 min apart, with no missing frames. Missing frames are associated with the failure of the NWCSAF satellite retrieval and are spaced randomly in time. For example, if the 0515, 0530, and 0545 UTC frames are available on a given day then the 0600 UTC nowcast is possible; if, however, the 0845 UTC frame is missing on that day, then the 0900 UTC nowcast cannot be included. Thus, the number of possible nowcasts varies according to initialization time, and these are shown in Table 1. Data were considered from 1 November 2019 until 11 October 2020, and the number of nowcasts

TABLE 1. The number of possible nowcasts for each initialization time.

Initialization	No. of nowcasts
0000 UTC	253
0300 UTC	236
0600 UTC	199
0900 UTC	191
1200 UTC	230
1500 UTC	262
1800 UTC	256
2100 UTC	235

available per month is shown in Table 2. The CRR data are in the Network Common Data Form (netCDF) format (Unidata 2021) and, like Hill et al. (2020), we use the latest version of the NWCSAF CRR algorithm over a 1500 (east–west) \times 1200 (south–north) gridpoint domain. This covers from Cameroon in the southeast to Morocco in the northwest (see the domain in Figs. 2 and 4, described in more detail below).

3. Description of pySTEPS optical flow method

The nowcasting initiative pySTEPS (Pulkkinen et al. 2019a,b; GitHub 2020) is free, open-source, community-supported Python-based code that supports a variety of radar and satellite formats, and includes verification tools. The modular system allows several options to establish the motion of tracked features (discussed below). The work shown here uses pySTEPS version 1.4.1 with the optical flow technique. Essentially, this takes a sequence of images and, from the change in intensity between images, calculates the motion flow vectors. A key assumption of the optical flow method is that, for a given pixel at time t and position $x(t)$, $y(t)$ with intensity $I(x, y)$, the brightness constancy constraint equation holds:

$$\frac{\partial I}{\partial x}U + \frac{\partial I}{\partial y}V + \frac{\partial I}{\partial t} = 0, \quad (1)$$

where U and V are the optical flow velocity components in the x and y directions, respectively. For two successive images at a given target pixel, the spatial derivatives of the intensities can be calculated, as can the time derivative of intensity (the difference between frames). This leaves (1) with two unknowns, U and V , resulting in an underdetermined system. The Lucas–Kanade approach (Lucas and Kanade 1981; OpenCV 2021) assumes that the pixels immediately surrounding the target pixel all move together. Thus, taking the nearest neighbors to the target pixel, this would then produce nine equations in two unknowns—an overdetermined system. To resolve this, the least squares method is applied to find the best solution for U and V . The above method is ideally designed for situations in which features move slowly, ideally by one pixel. The pySTEPS implementation of Lucas–Kanade uses the “pyramid” method whereby the underlying data are subjected to various degrees of coarsening—this deals with cases in which features may move rapidly, that is, by more than one pixel (Bouquet 2000). As part of the Lucas–Kanade

TABLE 2. The number of possible nowcasts for each month.

Month and year	No. of nowcasts
Nov 2019	167
Dec 2019	188
Jan 2020	109
Feb 2020	84
Ma 2020	205
Apr 2020	174
May 2020	158
Jun 2020	188
Jul 2020	203
Aug 2020	188
Sep 2020	160
Oct 2020	38

implementation, the motion vectors are interpolated onto regions where there is no precipitation (OpenCV 2021)—the “dense” Lucas–Kanade algorithm. The Lucas–Kanade method was chosen for this study because it is conceptually simple and is also the fastest and least computationally intensive method (Pulkkinen et al. 2019b). It is worth mentioning that Pulkkinen et al. (2019b) found that the choice of optical flow method had a minimal effect on the skill of nowcasts they considered. Note that this method advects existing precipitation and does not create, or remove, precipitation.

The optical-flow-based nowcasting method is as follows:

- 1) A sequence of images (typically three), spaced equally and sequentially in time, is taken as the training data and is read into pySTEPS.
- 2) The Lucas–Kanade optical flow method is applied, and the motion vectors are determined.
- 3) The retrieved structures are propagated according to the constraints imposed by the temporal separation, the flow vectors, and the brightness constancy equation in (1). At this point (if historical data are used), the nowcast can be compared with retrievals and the skill level can be calculated.

We stress that all of the above procedures are routine (and routines) in pySTEPS, and no additional choices of parameters/options were made, other than selecting the Lucas–Kanade algorithm. Each 6-h nowcast used in this paper took, typically, 30 s to produce on a domestic laptop. No further tuning or use of ensembles/random noise has been included. This is so as to (i) lower the number of degrees of freedom and increase the generality and reproducibility of the study, (ii) determine the usefulness of the method in its “base state,” and (iii) provide a benchmark against which future modifications to the method may be evaluated.

4. Verification

PySTEPS includes a suite of verification algorithms (Pulkkinen et al. 2019b). In this study, the fractions skill score (FSS) is used (Roberts and Lean 2008). The FSS method is designed to provide a verification at different spatial scales and at different rain rates. This is a nearest-neighbor type approach. For each pixel

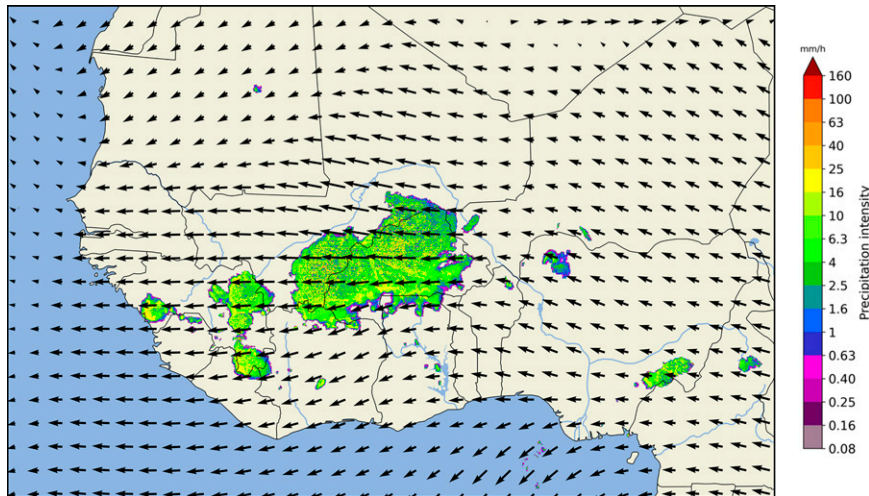


FIG. 1. The motion vectors for the 0000 UTC 15 Aug 2020 nowcast. For purposes of clarity, motion vectors are shown every 40 grid points. CRR is also shown at lead time = 0 h.

in the domain, surrounding points within a given square of physical length L , in kilometers, (hereinafter referred to as the “scale”) are considered. The number of rain points in the nowcast square is compared with the number of rain points in the corresponding observed (or in this case, retrieved) square. This is done for every pixel, and a skill metric is constructed that depends upon the length scale L . When there is no rain in both the nowcast (or equivalently, the last frame of the training data) and the corresponding CRR frame in the verification, then the FSS is undefined. For full details, see Roberts and Lean (2008).

In this approach a nowcast may have low skill at small scales but reasonable skill at larger scales. From another perspective: given a level of skill required, this effectively selects the scale at which this is possible. We have considered scales of 8, 16, 32, 64, 128, and 256 km. The FSS is an appropriate measure for the West African region. Although a nowcast having skill at small scales would be highly desirable, a nowcast that has skill at larger scales is welcome and useful also, in view of the difficulties facing forecasters in this region. The FSS is a standard module in pySTEPS, and using this metric is helpful for potential users who may have limited software/computing facilities.

Typically, the threshold for a useful forecast is taken to be $FSS > 0.5$. From Roberts and Lean (2008) a more appropriate target for a useful FSS is $FSS > 0.5 + f_0/2$ where f_0 is the fractional coverage of CRR (i.e., the proportion of pixels in the domain where $CRR > 0$). This is halfway between a random forecast and a forecast with perfect skill. Thus, in general, the target for a useful forecast threshold will be slightly higher than 0.5. For ease of interpretation, all FSS referred to from now on will have the fractional coverage factor subtracted, and so the useful forecast threshold in what follows can be taken to be 0.5.

In this study the CRR data have been used as both training (providing the motion vectors) and verification fields. Ideally, verification would be performed against an independent

dataset, such as rain gauge data. Such data are sparse—see, for example, the report of the World Meteorological Organization Systematic Observations Financing Facility (SOFF 2021), making such a verification unfeasible. Verification against NWP was thought to be problematic, due to the challenges associated with NWP in this region (see section 1 above). Given that Hill et al. (2020) showed that CRR has useful skill in both retrieval and extrapolation, the CRR data were used as the validation dataset. Thus, in what follows, we are (in strict terms) assessing the skill of the extrapolation algorithm and not the value of the underlying CRR product. The CRR data have inherent problems, as discussed above (section 2). Further work is needed for an independent verification of the ability of CRR to capture true rainfall rates, and the authors are investigating this.

5. Results

a. Example nowcasts

Figures 1 and 2 show the motion vectors and retrieved and nowcast CRR fields at various lead times for the 15 August 2020 at 0000 UTC. In this example there is little or no growth of convection and the large structure seen over central West Africa propagates somewhat south of westward across the continent at a near-constant velocity (see the retrieved rain rates in Figs. 2a–c). As can be seen from the motion vectors, this structure is stretched in the north–south direction, and the resulting nowcast structure is larger than that in the retrieval. Although there is some observed decay in this feature after 6 h, the nowcast CRR envelops the retrieved CRR. In this example, the optical flow method captures the observed motion very well. For *all* scales considered (8–256 km), the FSS never falls below 0.6 at a threshold of 1 mm h^{-1} , even at 6-h lead time. This was the best nowcast (in terms of FSS) of all those included in this study. To give some context, the mean of all nowcasts at 6-h lead time and a

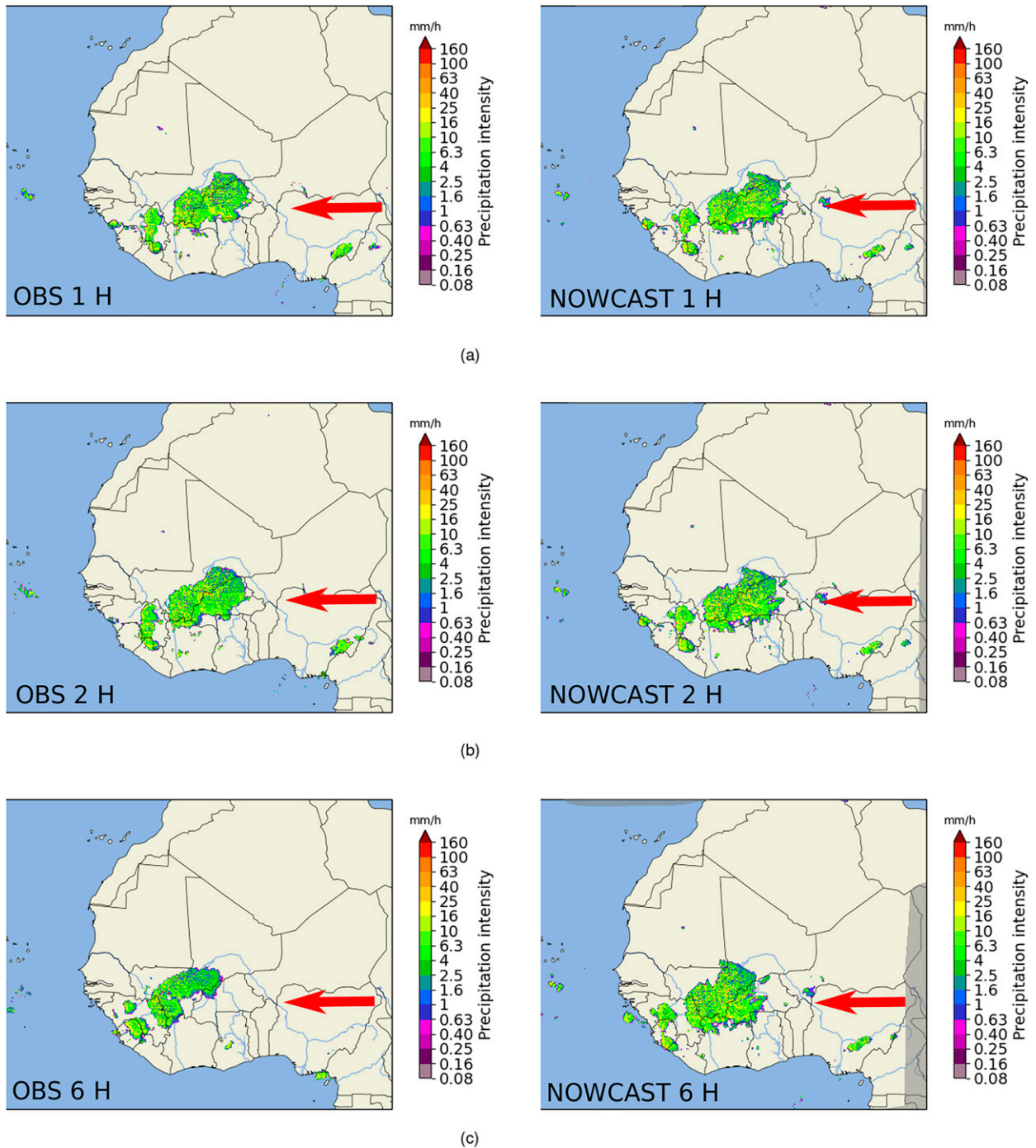


FIG. 2. An example of a good nowcast, 0000 UTC 15 Aug 2020: (left) the observed (i.e., satellite retrieved) CRR and (right) corresponding nowcasts for (a) 1-, (b) 2-, and (c) 6-h lead time. Note the shaded area in (c), where data are not available (since the flow is east-west, indicated by the red arrow).

scale of 8 km was between 0.15 and 0.25 (see Fig. 5 below and related discussion).

In contrast, several days later at 1200 UTC 18 August 2020, the nowcast is relatively poor (Figs. 3 and 4). After 1 h the retrieved and nowcast CRR bear some resemblance. After

2 h, convective intensification is apparent in the retrievals. Although the detected winds are broadly similar to those in Fig. 1, the subsequent widespread initiation and growth of convection apparent after 6 h caused a disparity between the retrievals and the nowcast. In this case, even after 2 h, the

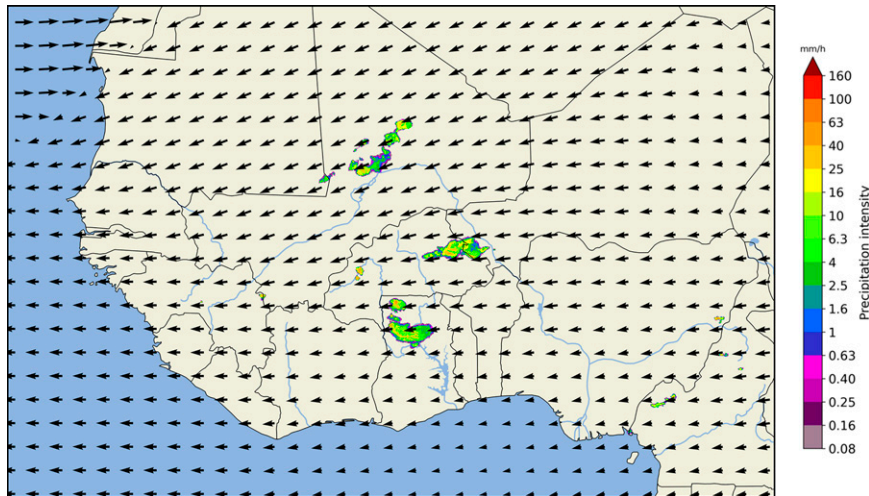


FIG. 3. As in Fig. 1, but for the 1200 UTC 18 Aug 2020 nowcast.

FSS is less than 0.5 for all scales, because the optical flow method cannot capture the growth and initiation of convection (see section 3). The CRR rain-rate retrieval algorithm does not perform as well at nighttime, as mentioned in section 2. However, any deficiencies would apply equally to all times in this nowcast, and so the results here are at least self-consistent: we are not comparing with an independent measurement (e.g., rain gauges). Note, however, that a forecaster in an operational setting would not look at this type of plot in isolation. A forecaster would use it in combination with other satellite and NWP products. Given the time of year and time of day, in combination with the observed initiation of deep convection and widespread high convective available potential energy, a forecaster would certainly expect a significant risk of these small cells growing to larger organized systems, and of further initiation, as is in fact observed.

The above “good” and “poor” nowcasts were selected as extreme cases of the nowcasting performance, and the majority of nowcasts lie somewhere between these two extremes. This can be shown by examining the statistics of the available nowcasts. As seen above the method can produce variable results depending upon the amount of convective genesis and/or growth. Thus, evaluating the method over many successive instances will demonstrate both the general applicability of the method and will highlight any diurnal/seasonal variations in FSS.

b. FSS statistics

Figure 5 shows the mean and standard error of FSS, separated by initialization time, for the small (8 km) and larger (64 km) scales. There is mean skill greater than 0.5 out to about 90 min for 8-km scale and to about 2.5 h for 64-km scale. This scale dependence is explored further in the next section.

There is a significant diurnal signal in the FSS, with the lowest FSS being associated with an initialization time of 1500 UTC. The prevalence of convective initiation/growth from 1500 UTC onward is responsible for reducing the skill for this initialization time (Duvel 1988; Mohr 2004; Laing et al. 2011; Crook et al. 2019). This is confirmed by the 1200 UTC

initialization nowcast, which starts off with similar skill to the other earlier initializations, then becomes poorer after 3 h, that is, after 1500 UTC. At the 64-km scale, the 1200 UTC nowcast recovers somewhat toward the end of the nowcast. For both the 8- and 64-km scales, the 1800 UTC nowcast behaves similarly to the better-performing nowcasts. This is consistent with the most intense period of convective initiation, in the period 1500–1800 UTC. In contrast, convection-permitting NWP can give their best performance at these times (see, e.g., Woodhams et al. 2018). This is also the time of day when the land surface is most predictable (Klein and Taylor 2020).

The standard errors of the mean in Fig. 5 show that the nowcasts initialized at 1500 UTC are lower than those initialized at other times of day. This can be seen in the fact that the means for the 1500 UTC initialization are, for lead times greater than 45 min, not contained within the error bars of any other initialization time, suggesting a statistically significant difference.

If used operationally, there would be no simple means to estimate the likelihood that a given nowcast has skill—so FSS distribution plots can be constructed to show the probability of obtaining a useful forecast based upon a given rain rate threshold and a given feature scale. For example, Fig. 6 displays the distribution for 1 mm h^{-1} threshold and at a scale of 8 km. It can be seen that there is a 50% chance that the FSS will be higher than 0.5 at a lead time of between 1 and 2 h.

If we define a lead-time metric $T_i(p, s)$ where s is the feature scale (km) and p is the percentage of nowcasts with $\text{FSS} \geq 0.5$, then $T_i(51, s)$ will give a lead time for which the majority of nowcasts had at least a skill score of 0.5—this is the lead time for which the majority of nowcasts were useful. For brevity, we denote this by $T_Y(s)$. In practice, because the frames are separated in time by discrete amounts of 15 min, and it is unlikely that the FSS at a given time is exactly 0.5, $T_Y(s)$ is calculated as the mean of average of the longest lead time for which the condition is not satisfied and the shortest lead time for which the condition is satisfied. Values of this useful lead time are shown in Fig. 7 for several FSS thresholds. Overall, the figure shows useful skill at around 3 h for a

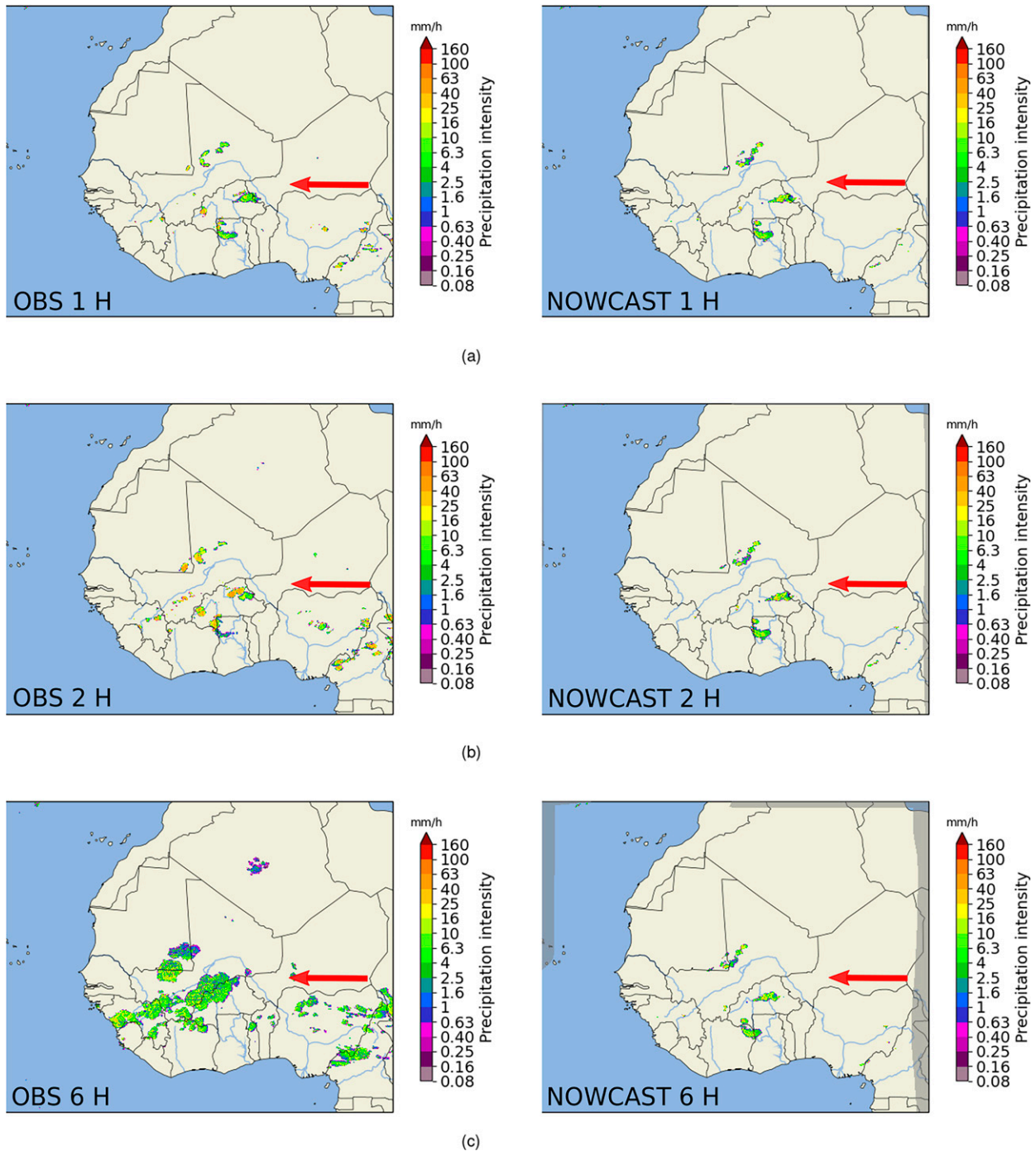


FIG. 4. As in Fig. 2, but for an example of a poor nowcast, 1200 UTC 18 Aug 2020.

64-km scale for thresholds of 1–10 mm h^{-1} . For a 256-km scale, Useful skill is over 4 h (for thresholds of 1 and 5 mm h^{-1}), and over 3.5 h for a threshold of 10 mm h^{-1} .

c. Comparison with NWCSAF extrapolations

As mentioned in section 2, NWCSAF already provide extrapolations of CRR. In this section we compare the

NWCSAF extrapolations with the present pySTEPS extrapolations. As in Hill et al. (2020), 90-min extrapolations are considered.

As before, the dataset is limited by completeness (not all 90-min, uninterrupted NWCSAF nowcasts were present in the catalog)—a total of 765 synchronized pySTEPS and NWCSAF nowcasts were available. To compare these two

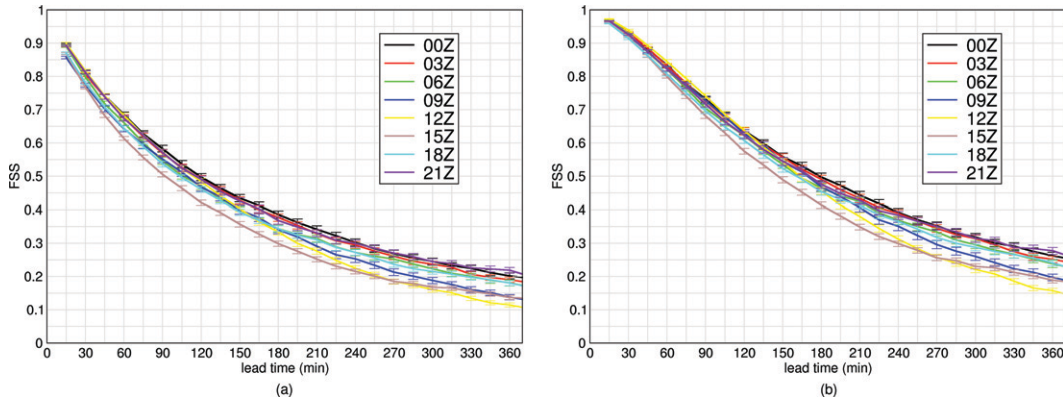


FIG. 5. FSS as a function of lead time for a feature scale of (a) 8 and (b) 64 km and for various initialization times (see legend). Error bars display the standard error of the mean.

datasets, the NWCSAF extrapolations were processed by the pySTEPS verification module (i.e., the motion advection step was omitted). In general, the FSS for pySTEPS (denoted by FSS_p) and the FSS for NWCSAF (FSS_N) are very similar for the 90-min lead-time period. However, there are differences, with FSS_p being generally higher than FSS_N .

Denote the difference between any two given nowcasts as $\Delta_{FSS} = FSS_p - FSS_N$. Figure 8 shows the percentage of all cases for which $\Delta_{FSS} > 0$ for a scale of 8 km and a threshold of 1 mm h^{-1} , and for the range of initialization times. The apparent trend is for NWCSAF to perform similarly to pySTEPS at the first 15-min nowcast but subsequently the pySTEPS nowcasts have higher skill. The majority of pySTEPS nowcasts have higher skill for all initialization times for lead times greater than or equal to 30 min. There are differences in response between the initialization times—for example, the percentage of cases where $\Delta_{FSS} > 0$ is greater for 1200 UTC than for 0900 and 1500 UTC.

It is not clear why this is the case, and without further detailed knowledge of the NWCSAF algorithm, it is not possible to say. One possible explanation may be the difference in

data used to calculate the atmospheric motion vectors. The NWCSAF algorithm identifies “tracers” (features) in up to seven SEVIRI channels (Pereda 2019). The atmospheric motion vectors are determined by the advection of these tracers in successive retrievals, as described in section 2. The slight difference in skill between pySTEPS and NWCSAF extrapolations might be explained by the fact that pySTEPS identifies features in one field only—a derived product (CRR).

Values of Δ_{FSS} themselves are shown in Fig. 9. Consistent with the above, the differences between the two approaches are negligible at 15 min (with a tendency for negative Δ_{FSS} at this time) but after that Δ_{FSS} is positive and increases linearly (approximately) with time for all initialization times. The rate of increase of Δ_{FSS} is approximately constant across all initialization times. After 90 min, Δ_{FSS} is typically 0.04. Further work would be needed to determine the precise reasons for these small differences between the pySTEPS and NWCSAF approaches.

In summary, it can be said that the optical flow method with no enhancements performs as well as (and usually has

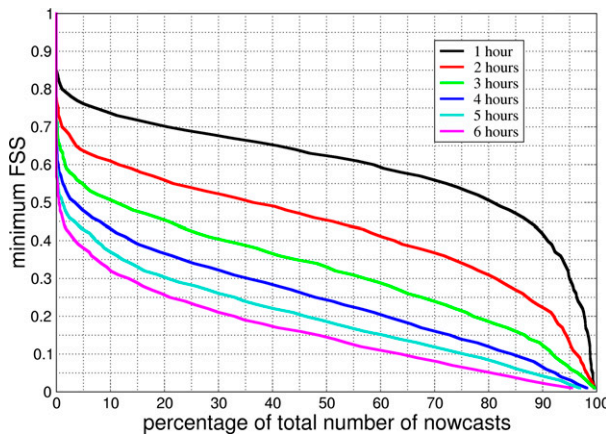


FIG. 6. The percentage of nowcasts having a given FSS minimum for various lead times. The feature scale is 8 km.

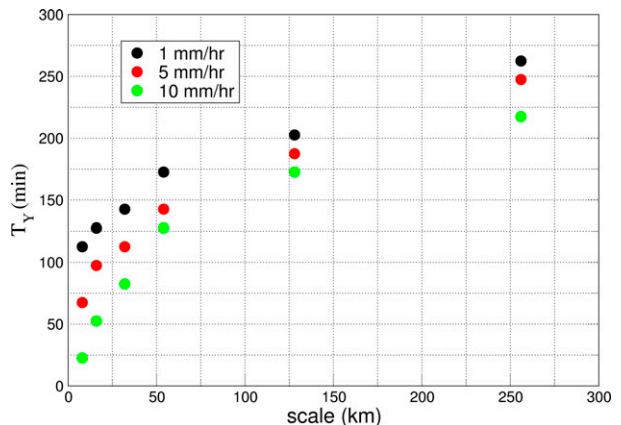


FIG. 7. The dependence of useful forecast time $T_Y(s)$ upon scale size, for scales of 8, 16, 32, 64, 128, and 256 km. FSS thresholds are shown in different colors.

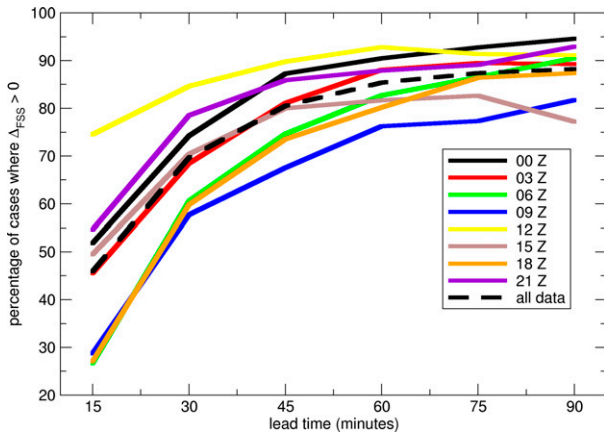


FIG. 8. The number of cases for which the pySTEPS FSS (FSS_P) is greater than the NWCSAF FSS (FSS_N) as a function of lead time, for various initialization times. The dashed black line is the mean of all cases.

more skill than) the NWCSAF extrapolation, especially for lead times greater than 15–30 min.

6. Summary

PySTEPS with optical flow has been applied to satellite-derived CRR over West Africa. Particularly good nowcasts can be achieved when there is little initiation or growth of convection and rainfall changes at a given location are due to the horizontal motion of existing storms. Extrapolation-based nowcasting is less skillful when initiation and growth are strong.

We have shown that useful nowcasts can be produced, typically up to ~2 h on the smallest scales (on the order of 10 km) at 1 mm h^{-1} and over ~4 h on the larger scales (on the order of 200 km) at 5 mm h^{-1} . For thresholds of 10 mm h^{-1} , useful forecasts can be produced up to 3.5-h lead time at the larger scales.

At all scales studied, there was diurnal cycle evident in the FSS. With very few exceptions, the worst-performing 6-h nowcasts are those that are initialized at 1200 and 1500 UTC: this is the time of day when development and growth of new convective cells is at its daily maximum, and this behavior is not captured in the optical flow method.

Comparison with NWCSAF 90-min extrapolations shows a good agreement, with pySTEPS nowcasts having generally higher FSS than the NWCSAF nowcasts. The use of the method, without further intervention or additional data, shows that there could be a potential to use pySTEPS for operational nowcasting over West Africa. Such work as presented here could supplement existing products used by forecasters in Africa. Further tuning may be possible, either to pySTEPS algorithms, or via the addition of NWP products. While this is beyond the scope of this short note, the authors intend to investigate this in future work. In addition, we have not compared the extrapolation skill with that of NWP or with higher-quality rainfall data as in Hill et al. (2020), and we are actively pursuing this as a further means to characterize the potential benefit of this work.

Given the difficulties facing NWP for Africa and the general unpredictability of convective storms, nowcasting solutions are urgently needed, and African forecast centers are beginning to use satellite-based nowcasting to provide alerts to stakeholders (Roberts et al. 2021). In this paper we have been able to demonstrate extrapolation of satellite-derived

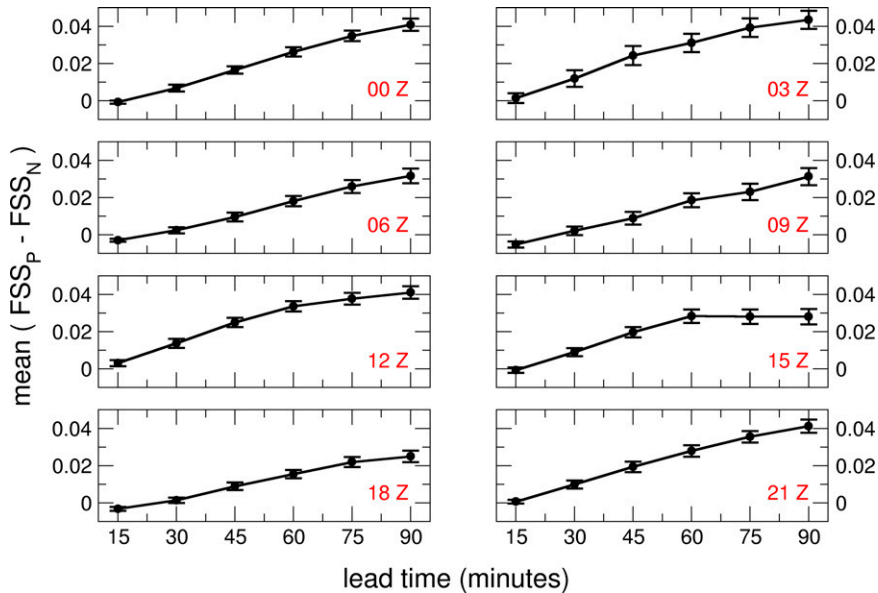


FIG. 9. The mean difference between FSS_P and FSS_N as a function of lead time, for various initialization times (labeled in red text). The error bars denote the standard error of the mean.

CRR in a nowcasting algorithm for West Africa. These extrapolations can have useful skill for at least 2 h and even 4 h on larger scales, using a standard forward projection algorithm. We are currently working to implement these solutions and provide products and tools to the African weather services.

Acknowledgments. This work was supported by U.K. Research and Innovation as part of the Global Challenges Research Fund, African SWIFT program, Grant NE/P021077/1, led by the National Centre for Atmospheric Science (NCAS). Zhiqiang Cui is partly funded by the Centre for Environmental Modelling and Computation, University of Leeds. We are extremely grateful to the three reviewers of the initial version of this paper for their close reading of the paper, their helpful comments, and constructive criticisms and suggestions.

Data availability statement. pySTEPS is open-source software (<https://pysteps.github.io/>).

REFERENCES

- Batrick, B., and J. Mort, 1981: Nowcasting: Mesoscale observations and short-range prediction: Proceedings of an International Symposium, 25–28 August 1981, Hamburg, Germany. European Space Agency SP-165, 415 pp.
- Bedka, K., J. Brunner, R. Dworak, W. Feltz, J. Otkin, and T. Greenwald, 2010: Objective satellite-based detection of overshooting tops using infrared window channel brightness temperature gradients. *J. Appl. Meteor. Climatol.*, **49**, 181–202, <https://doi.org/10.1175/2009JAMC2286.1>.
- Birkenheuer, D. L., 1987: Integration of satellite data with other data for nowcasting. *Adv. Space Res.*, **7**, 363–373, [https://doi.org/10.1016/0273-1177\(87\)90343-7](https://doi.org/10.1016/0273-1177(87)90343-7).
- Bouguet, J.-Y., 2000: Pyramidal implementation of the Lucas Kanade feature tracker. Intel Corporation Doc., 9 pp.
- Bowler, N. E., C. E. Pierce, and A. W. Seed, 2006: Steps: A probabilistic precipitation forecasting scheme which merges an extrapolation nowcast with downscaled NWP. *Quart. J. Roy. Meteor. Soc.*, **132**, 2127–2155, <https://doi.org/10.1256/qj.04.100>.
- Browning, K. A., Ed., 1982: *Nowcasting*. Academic Press, 256 pp.
- Crook, J., C. Klein, S. Folwell, C. M. Taylor, D. J. Parker, R. Stratton, and T. Stein, 2019: Assessment of the representation of west African storm lifecycles in convection-permitting simulations. *Earth Space Sci.*, **6**, 818–835, <https://doi.org/10.1029/2018EA000491>.
- de Coning, E., M. Gijben, B. Maseko, and L. van Hemert, 2015: Using satellite data to identify and track intense thunderstorms in South and southern Africa. *S. Afr. J. Sci.*, **111**, 1–5, <https://doi.org/10.17159/sajs.2015/20140402>.
- Duvel, J. P., 1988: Analysis of diurnal, interdiurnal and interannual variations during Northern Hemisphere summers using Meteosat infrared channels. *J. Climate*, **1**, 471–484, [https://doi.org/10.1175/1520-0442\(1988\)001<0471:AODIAI>2.0.CO;2](https://doi.org/10.1175/1520-0442(1988)001<0471:AODIAI>2.0.CO;2).
- EUMETSAT, 2021: EUMETSAT Satellite Application Facility on Climate Monitoring. Accessed 3 March 2021, https://www.cmsaf.eu/EN/Overview/Overview_node.html.
- Gijben, M., and E. De Coning, 2017: Using satellite and lightning data to track rapidly developing thunderstorms in data sparse regions. *Atmosphere*, **8**, 67, <https://doi.org/10.3390/atmos8040067>.
- GitHub, 2020: pySTEPS. GitHub, accessed 3 March 2021, <https://pysteps.github.io/>.
- Golding, B. W., 1998: Nimrod: A system for generating automated very short range forecasts. *Meteor. Appl.*, **5**, 1–16, <https://doi.org/10.1017/S1350482798000577>.
- Hernanz, A., and J. A. Lahuerta, 2019: Algorithm theoretical basis document for the precipitation product processors of the NWC/GEO. EUMETSAT NWCSAF Rep., 75 pp., https://www.nwcsaf.org/Downloads/GEO/2018/Documents/Scientific_Docs/NWC-CDOP2-GEO-AEMET-SCI-ATBD-Precipitation_v2.1.pdf.
- Hill, P. G., T. H. Stein, A. J. Roberts, J. K. Fletcher, J. H. Marsham, and J. Groves, 2020: How skilful are nowcasting satellite applications facility products for tropical Africa? *Meteor. Appl.*, **27**, e1966, <https://doi.org/10.1002/met.1966>.
- Jann, A., 2017: User manual for the extrapolated imagery processor of the NWC/GEO: Science part. ZAMG Doc., 22 pp., https://www.nwcsaf.org/AemetWebContents/ScientificDocumentation/Documentation/GEO/v2016/NWC-CDOP2-GEO-ZAMG-SCI-UM-EXIM_v1.0.pdf.
- Judt, F., 2020: Atmospheric predictability of the tropics, middle latitudes, and polar regions explored through global storm-resolving simulations. *J. Atmos. Sci.*, **77**, 257–276, <https://doi.org/10.1175/JAS-D-19-0116.1>.
- Klein, C., and C. M. Taylor, 2020: Dry soils can intensify mesoscale convective systems. *Proc. Natl. Acad. Sci. USA*, **117**, 21 132–21 137, <https://doi.org/10.1073/pnas.2007998117>.
- Kniffka, A., and Coauthors, 2020: An evaluation of operational and research weather forecasts for southern West Africa using observations from the DACCWA field campaign in June–July 2016. *Quart. J. Roy. Meteor. Soc.*, **146**, 1121–1148, <https://doi.org/10.1002/qj.3729>.
- Laing, A. G., R. E. Carbone, and V. Levizzani, 2011: Cycles and propagation of deep convection over equatorial Africa. *Mon. Wea. Rev.*, **139**, 2832–2853, <https://doi.org/10.1175/2011MWR3500.1>.
- Lebedev, V., and Coauthors, 2019: Precipitation nowcasting with satellite imagery. *Proc. 25th ACM SIGKDD Int. Conf. on Knowledge Discovery and Data Mining*, Anchorage, AK, Association for Computing Machinery, 2680–2688, <https://doi.org/10.1145/3292500.3330762>.
- Line, W., T. Schmit, D. Lindsey, and S. Goodman, 2016: Use of geostationary super rapid scan satellite imagery by the storm prediction center. *Wea. Forecasting*, **31**, 483–494, <https://doi.org/10.1175/WAF-D-15-0135.1>.
- Lucas, B. D., and T. Kanade, 1981: An iterative image registration technique with an application to stereo vision. *IJCAI'81: Proc. 7th Int. Joint Conf. on Artificial Intelligence*, Vol. 2, Vancouver, BC, Canada, International Joint Conferences on Artificial Intelligence, 674–679, <http://dl.acm.org/citation.cfm?id=1623264.1623280>.
- Maranan, M., A. H. Fink, and P. Knippertz, 2018: Rainfall types over southern West Africa: Objective identification, climatology and synoptic environment. *Quart. J. Roy. Meteor. Soc.*, **144**, 1628–1648, <https://doi.org/10.1002/qj.3345>.
- Marsham, J. H., N. S. Dixon, L. Garcia-Carreras, G. M. S. Lister, D. J. Parker, P. Knippertz, and C. E. Birch, 2013: The role of moist convection in the West African monsoon system: Insights from continental-scale convection-permitting simulations. *Geophys. Res. Lett.*, **40**, 1843–1849, <https://doi.org/10.1002/grl.50347>.

- Mecikalski, J., and K. Bedka, 2006: Forecasting convective initiation by monitoring the evolution of moving cumulus in daytime goes imagery. *Mon. Wea. Rev.*, **134**, 49–78, <https://doi.org/10.1175/MWR3062.1>.
- Mohr, K. I., 2004: Interannual, monthly, and regional variability in the wet season diurnal cycle of precipitation in sub-Saharan Africa. *J. Climate*, **17**, 2441–2453, [https://doi.org/10.1175/1520-0442\(2004\)017<2441:IMARVI>2.0.CO;2](https://doi.org/10.1175/1520-0442(2004)017<2441:IMARVI>2.0.CO;2).
- NWCSAF, 2020: Welcome to the NWC SAF. Accessed 3 March 2021, <https://www.nwcsaf.org/>.
- OpenCV, 2021: Optical flow. Accessed 3 March 2021, https://docs.opencv.org/3.4/d4/dee/tutorial_optical_flow.html.
- Otsuka, S., S. Kotsuki, M. Ohhigashi, and T. Miyoshi, 2019: GSMaP RIKEN nowcast: Global precipitation nowcasting with data assimilation. *J. Meteor. Soc. Japan*, **97**, 1099–1117, <https://doi.org/10.2151/jmsj.2019-061>.
- Pereda, J. G., 2019: Algorithm theoretical basis document for the wind product processor of the NWC/GEO. EUMETSAT NWCSAF Rep., 108 pp., https://www.nwcsaf.org/Downloads/GEO/2018.1/Documents/Scientific_Docs/NWC-CDOP2-GEO-AEMET-SCI-ATBD-Wind_v2.2.pdf.
- Pulkkinen, S., D. Nerini, A. A. Pérez Hortal, C. Velasco-Forero, A. Seed, U. Germann, and L. Foresti, 2019a: Pysteps—A community-driven open-source library for precipitation nowcasting. *3rd European Nowcasting Conf.*, Madrid, Spain, EUMETNET, P18, <https://edrop.zamg.ac.at/owncloud/index.php/s/9tiKLz9JFisqPCP?path=%2FPOSTERS#pdfviewer>.
- , —, —, —, —, —, and —, 2019b: Pysteps: An open-source python library for probabilistic precipitation nowcasting (v1.0). *Geosci. Model Dev.*, **12**, 4185–4219, <https://doi.org/10.5194/gmd-12-4185-2019>.
- Roberts, A. J., and Coauthors, 2022: Nowcasting for Africa: Advances, potential and value. *Weather*, <https://doi.org/10.1002/wea.3936>, in press.
- Roberts, N. M., and H. W. Lean, 2008: Scale-selective verification of rainfall accumulations from high-resolution forecasts of convective events. *Mon. Wea. Rev.*, **136**, 78–97, <https://doi.org/10.1175/2007MWR1213.1>.
- SEVIRI, 2021: The Spinning Enhanced Visible and InfraRed Imager (SEVIRI) is MSG's primary instrument and has the capacity to observe the Earth in 12 spectral channels. SEVIRI, accessed 3 March 2021, <https://www.eumetsat.int/seviri>.
- Shi, X., Z. Gao, L. Lausen, H. Wang, D.-Y. Yeung, W.-K. Wong, and W.-C. Woo, 2017: Deep learning for precipitation nowcasting: A benchmark and a new model. *Advances in Neural Information Processing Systems*, I. Guyon et al., Eds., Curran Associates, Inc., 11 pp., <https://proceedings.neurips.cc/paper/2017/file/a6db4ed04f1621a119799fd3d7545d3d-Paper.pdf>.
- Sieglaff, J., D. Hartung, W. Feltz, L. Crounce, and V. Lakshmanan, 2013: A satellite-based convective cloud object tracking and multipurpose data fusion tool with application to developing convection. *J. Atmos. Oceanic Technol.*, **30**, 510–525, <https://doi.org/10.1175/JTECH-D-12-00114.1>.
- SOFF, 2021: The gaps in the Global Basic Observing Network (GBON). SOFF Doc., 8 pp., https://library.wmo.int/doc_num.php?explnum_id=10377.
- Thiery, W., L. Gudmundsson, K. Bedka, F. H. M. Semazzi, S. Lhermitte, P. Willems, N. P. M. van Lipzig, and S. I. Seneviratne, 2017: Early warnings of hazardous thunderstorms over Lake Victoria. *Environ. Res. Lett.*, **12**, 074012, <https://doi.org/10.1088/1748-9326/aa7521>.
- Unidata, 2021: Network Common Data Form (NetCDF). Unidata, accessed 3 March 2021, <https://www.unidata.ucar.edu/software/netcdf/>.
- UNOCHA, 2020: West and Central Africa: Flooding situation as of 25 September 2020. UNOCHA, accessed 3 March 2021, <https://reliefweb.int/report/niger/west-and-central-africa-flooding-situation-25-september-2020>.
- Vogel, P., P. Knippertz, A. H. Fink, A. Schlueter, and T. Gneiting, 2018: Skill of global raw and postprocessed ensemble predictions of rainfall over northern tropical Africa. *Wea. Forecasting*, **33**, 369–388, <https://doi.org/10.1175/WAF-D-17-0127.1>.
- , —, —, —, and —, 2020: Skill of global raw and postprocessed ensemble predictions of rainfall in the tropics. *Wea. Forecasting*, **35**, 2367–2385, <https://doi.org/10.1175/WAF-D-20-0082.1>.
- Wang, Y., and Coauthors, 2017: Guidelines for nowcasting techniques. World Meteorological Organization Doc. WMO-1198, 67 pp., https://library.wmo.int/doc_num.php?explnum_id=3795.
- Woo, W.-C., and W.-K. Wong, 2017: Operational application of optical flow techniques to radar-based rainfall nowcasting. *Atmosphere*, **8**, 48, <https://doi.org/10.3390/atmos8030048>.
- Woodhams, B. J., C. E. Birch, J. H. Marsham, C. L. Bain, N. M. Roberts, and D. F. A. Boyd, 2018: What is the added value of a convection-permitting model for forecasting extreme rainfall over tropical East Africa? *Mon. Wea. Rev.*, **146**, 2757–2780, <https://doi.org/10.1175/MWR-D-17-0396.1>.
- Žagar, N., 2017: A global perspective of the limits of prediction skill of NWP models. *Tellus*, **69A**, 1317573, <https://doi.org/10.1080/16000870.2017.1317573>.